SAND2021-16070C

Evaluating the Thermal Efficiency of Multistage Falling Particle Receivers Subject to Wind

Jae Bok Lee [(a)] and Brantley Mills

Sandia National Laboratories, P.O. Box 5800, MS-0836, Albuquerque, NM 87185-0836, USA

[(a)]Corresponding author: stlee@sandia.gov

Abstract. The thermal performance of a multistage falling particle receiver (MFPR) has been evaluated for a candidate utility-scale 100 MW_e particle-based concentrating solar power plant using a multi-physics computational fluid dynamics model. The present model accounts for incident solar radiation from the heliostats, particle dynamics, heat transfer, turbulent air flows, and environmental effects like wind. All simulations were performed using realistic operating and environmental parameters. In this study, the efficiency of a 2-stage MFPR has been explored for various geometrical parameters such as the trough heights and trough lengths. The best performing MFPR geometry provided a thermal efficiency of 88% in quiescent conditions. This design was evaluated for three separate wind speeds (5, 10, and 15 m/s), seven different wind directions (N, NNW, NW, WNW, W, and SW), and two different incident solar power (100 and 200 MW). Simulation results showed that the thermal efficiency is significantly affected by the wind direction. A correlation of MFPR efficiency as a function of the wind speed, wind direction, and incident solar power was developed with an R-squared value of ~0.94 indicating that the correlation may be effectively used to predict the thermal efficiency of 100 MW_e MFPRs in system models.

INTRODUCTION

Particle-based concentrating solar power (CSP) plants are a promising candidate for next generation CSP energy production since it can be coupled with high-efficiency power cycles such as supercritical CO_2 or air Brayton cycles to provide cost-effective and dispatchable electricity on demand. Solid particles (ceramic or sand) provide many advantages over conventional heat transfer media (e.g. steam, molten salts, etc.) due to their ability to reach higher temperatures (>1000°C) with direct storage and to be heated directly from concentrated sunlight [1]. Considerable efforts have been made to enhance the system-level net performance to achieve the target levelized cost of electricity (LCOE) of $0.05/kWh. Recent studies have shown that improving the falling particle receiver (FPR) efficiency makes a significant contribution to lowering LCOE [2]. Therefore, this paper focuses on improving the FPR efficiency to achieve target LCOE for system-level models.

The ability to scale up the FPR technology to commercial scales (>100 MW_e) is an important consideration for widespread CSP deployment. Numerical studies have been performed to investigate the thermal performance of FPRs at commercial scales, including both north-facing and face-down configurations. Khalsa *et al.* [3] observed that commercial scale particle receiver provided a thermal efficiency of up to 72.3% for the north-facing receiver and 78.9% for the face-down receiver, respectively. They observed that the north-facing receiver could yield a higher particle equilibrium temperature at the outlet although the thermal efficiency was lower than that with face-down receiver. Other face-down receiver designs were found to provide a higher thermal efficiency of up to ~87% [4].

Despite great potential, FPRs up to commercial scale (>100 MW_e) may be subject to degradation in the thermal performance from inherent properties of the concept. As falling particles are accelerated by gravity, the volume fraction of falling particles decreases with increasing size of receiver cavity. Low volume fractions increase the transmittance of the particle curtain, and thus the resulting solar energy absorbed by the particle curtain decreases. Furthermore, as particles are falling through larger dimensions of a receiver cavity, particle curtains may become unstable and dispersive due to increasing particle Reynolds number. Another concern for commercial scale FPRs is

the energy loss from advection. A large portion of energy loss comes from the advective losses due to buoyancy-driven flow generated from the temperature difference between the ambient air and air inside the receiver cavity [5]. The generated flow removes the energy from the particle curtain, and it escapes out of the cavity through the open aperture. Increasing the size of a FPR requires increasing the size of the aperture, which could significantly increase advective losses.

The performance degradation from advective losses can be more significant when considering external winds [6]. A previous study pointed out that wind blowing in parallel to the aperture of face-down receivers forms vortices that can create a condition where cooler air is entrained into the receiver cavity intensifying the advective loss [4]. A more recent computational study on north-facing receivers investigated advective losses under various wind directions and speeds [5]. The authors revealed that the wind direction is more significant to the augmentation of the advective loss compared to wind speeds. Mills *et al.* [7] also showed that the thermal efficiency can be substantially degraded by wind even at smaller pilot-plant scales (~1 MW_{th}). This implies that wind could have even more detrimental effects on the thermal efficiency as the size of a FPR increases, and thus the size of the aperture increases to commercial scales. Therefore, it is important to understand how the thermal efficiency is affected by the external wind, especially wind direction, and minimize the adverse effects of wind on a commercial scale FPR design.

Recently, much attention has been given to multi-stage concepts to overcome some drawbacks of FPRs. Ho *et al.* [8, 9] tested a method of obstructing particle flow using an array of porous mesh structures inserted to the particle receiver. The obstructed-flow design not only improved the particle residence time and particle heating, but also reduced the impacts of wind and particle loss through the aperture. Other studies adopted intermediate collecting troughs placed along the height of the receiver [10, 11]. The trough enabled reinitializing the particle velocity through the cavity such that the particle curtain could be more stable, and the energy absorbed by particles is enhanced with increasing residence time and volume fraction. The multi-stage concept also enables mixing of the particles in the multiple troughs to obtain uniform thermal distribution across the particle curtain [10]. In addition, an appropriate placement of multiple troughs can also mitigate the adverse effects from external winds by controlling cooler ambient air entering the receiver cavity [12]. Although a number of studies in multi-stage falling particle receiver (MFPR) have been performed, the quantification of commercial scale MFPR efficiency subject to external winds remains little understood. Moreover, it is necessary to define an efficient MFPR geometry can be designed at scale that surpasses the free-falling particle receiver (FFPR) efficiency.

Computational models can be utilized to aid in design efforts and to better predict the thermal performance of MFPRs in response to various wind conditions such as the wind speed and direction. However, to establish more accurate technoeconomic models, numerical modeling of the performance of MFPRs in ensemble conditions, regarding all relevant operating conditions mapped with wind effects, is needed. For a comprehensive parametric study, significant computational resources are required to obtain relationships of the thermal performance with relevant conditions. However, computational resources can be reduced by utilizing a correlation developed from more accurate computational models. In addition, a correlation allows for identifying which parameters are the most relevant to the thermal performance of a MFPR. This can provide an idea on which parameters should be controlled to achieve the target metrics for the system models.

In this study, a computational analysis is performed to quantify the thermal performance of MFPR for a candidate utility-scale 100 MW_e particle CSP plant using a computational fluid dynamics (CFD) model. The first goal of the present study is to obtain a MFPR design that provides higher efficiency compared to a similarly sized FFPR under the same operating conditions. The second goal is to investigate the MFPR efficiency in terms of the effective operating and environmental conditions. The third goal is to establish a robust correlation of the thermal efficiency with relevant operating and environmental parameters as defined for the simulations using the advanced CFD model. These efforts will guide future MFPR designs and confirm the targeted performance under realistic operating and external wind conditions at commercial scale.

The remainder of this paper is organized as follows. First, the computational model used to predict the thermal performance of the proposed 100 MW_e MFPR under various steady-state wind conditions is described. Then, MFPR efficiency with various trough lengths and trough heights in a quiescent condition is discussed. Then, the MFPR efficiencies for various wind speeds, wind directions, and incident solar powers are presented. Next, the results of this parametric study are used to generate correlations for the receiver performance as a function of the given parameters. Finally, the results of this study are summarized.

COMPUTATIONAL MODEL DESCRIPTION

The following section describes the computational models used to simulate the thermal performance of a MFPR for a candidate 100 MW_e particle CSP plant. This paper focuses primarily on the thermal performance of particle receiver(s) rather than other elements of the CSP plant such as storage tanks, heat exchanger, etc. This specific receiver design is part of a three-receiver concept on a single power tower where each receiver will receive approximately 200 MW_{th} peak of radiative energy. By simulating a single receiver, we are assuming its performance is unaffected by the neighboring receivers facing different azimuthal directions. A multi-physics CFD model was developed to evaluate the wind effects on MFPR performance in ANSYS Fluent® 2021 R1. The present model accounts for incident solar radiation, particle dynamics, heat transfer, turbulent air flows, and wind effects. All simulations are steady-state simulations and performed with realistic operating and environmental parameters.

The computational domain includes the air volume inside and outside the receiver geometry within a $L_x \times L_y \times L_z$ (=58m×55m×50m) as shown in Fig.1(a). The air continuum is modeled inside and outside the receiver to capture the buoyancy-driven air flows generated from the temperature difference between hot air inside the receiver cavity and the cold, denser ambient air. In this study, a converging tunnel leading to the receiver cavity, referred to as a SNOUT [7], is included to minimize the effects of wind at the aperture.

As a baseline, a FFPR geometry is modeled and discretized. A grid independence test was carried out to ensure that sufficient number of elements were used to simulate the included physical models. The receiver efficiency and thermal losses from advective/radiative effects were calculated for various number of elements as shown in Fig.2. Both the thermal losses and the receiver efficiency converged with an increasing number of elements. From this study, 3,008,286 tetrahedral cells were found to yield acceptable levels of accuracy with the full-physics model using the minimum number of elements as shown in Fig.2. As shown later, several MFPR geometries are modeled using the FFPR geometry as a baseline for various trough lengths and trough heights necessitating changes to the back wall of the receiver as well. However, each MFPR geometry is meshed using a similar element sizes and numbers to that for the FFPR. For reasonable comparison of thermal performance between MFPR and FFPR, the geometrical parameters irrelevant to multistage troughs (e.g. tunnel length, width of the receiver) were kept as constraints.

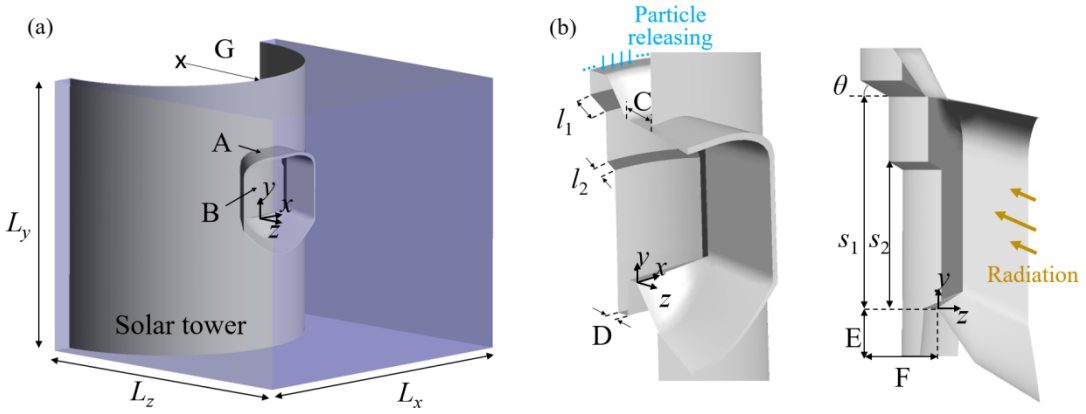

Item	Description	Item	Description
A	SNOUT	F	Cavity depth (=4m)
B	Aperture area (=144m^2)	G	Radius of solar tower (=50m)
C	Tunnel length	l_i	Lengths of i^{th} troughs
D	Hopper length	s_i	Heights of i^{th} troughs
E	Hopper depth (=4m)	θ	Angle of repose for particles

FIGURE 1. (a) Computational domain, (b) Representative MFPR geometry sliced by *y*-*z* plane (2-stages MFPR).

Lagrangian particles are released from the top of the receiver, as shown in Fig.1(b). CARBO HSP particles with chemical composition of 82% Al2O3, 7% Fe2O3, 5% SiO2, 3.5% TiO2 and a diameter of 350 μm are assumed in this study. Previous studies have shown that mass fractions in a falling particle curtain are typically below 10% [13]. With this regime of particle mass fraction, fluid-particle interactions are more dominant over particle-particle collisions. A

Eulerian-Lagrangian CFD model is utilized to simulate the particle-air interaction through drag forces and heat transfer occurring between parcels of particles and the air. The present study adopted the drag model proposed form Morsi and Alexander [14].

The realizable k-ε turbulence model was applied using Fluent's scalable wall functions that allows for a better approximation of fluid velocity near the wall. The wind is imposed as a velocity-inlet boundary condition where appropriate on the surrounding surfaces. Pressure-outlet boundary conditions are applied to the rest surfaces. A medium turbulence intensity of 5% and an eddy viscosity ratio of 10 were applied on inlet and outlet boundary surfaces to approximate turbulent boundary conditions as has been used in previous studies [4]. Thermal conduction through the Duraboard® receiver walls was modeled, and the receiver walls were convectively and radiatively coupled with the surrounding environment.

Elastic particle collisions with the walls were modeled, except with the hopper wall and intermediate troughs. The particles escaped the domain when they reached the hopper walls at the bottom of the receiver assuming particle bouncing in the hopper was negligible. With this strategy, convergence is improved and computational costs are reduced. More careful attention is needed for particles impacting the intermediate troughs. Particles are accumulated on the intermediate troughs, and the falling particles are impacting aggregate accumulations on each trough in steady-state. To mimic this behavior, the particle velocity is re-defined to a constant forward velocity upon collision with the trough mound. Specifically, the forward velocity is set to 0.3m/s with the angle of repose for CARBO HSP particles of θ=30$^{\mathbf{o}}$ that closely matches empirical observations of small-scale testing of the multi-stage concept [12].

A non-grey, discrete-ordinates (DO) radiation model was coupled with CFD model to model radiation from the heliostats and thermal emissions. The radiation spectrum was divided into three bands: 0.1-2.5 μm, 2.5-4.5 μm, 4.5-100 μm. The incident radiation from the heliostats enters entirely in the smallest wavelength band from a radiative boundary condition, while the two larger wavelength bands represent thermal emissions. The distinction in the two longer thermal bands accounts for the difference in the emissive properties of Duraboard® comprising the receiver walls. In this study, the air was modeled as a transparent, non-participating medium.

Solar radiation entering the computational domain is defined based on a compatible heliostat field for the 100 MW_e CSP plant. Using NREL's ray-tracing software, SolTrace, nine simulations are performed to compute an irradiation boundary condition for the DO model from different regions of the heliostat field at solar noon on the equinox. The radiation intensity and directionality from a particular section of the field on a plane 20m in front of the cavity aperture is computed for ~5×10^6 ray intersections. Using a 35×35 unit grid on that plane, the rays crossing that plane are locally averaged. Then, the resulting vectors are averaged and fit with analytical expressions to create functions that could easily be implemented into Fluent via a user defined function (UDF). These functions described the intensity, directionality, and beam spread variation across that plane for the DO model from each of the nine sections of the field. The cell faces on the north surface of the domain are then successively assigned contributions from different regions of the field, and the final intensity is scaled appropriately to achieve the desired radiative power. More details on ray-tracing model can be also found in the previous study [7].

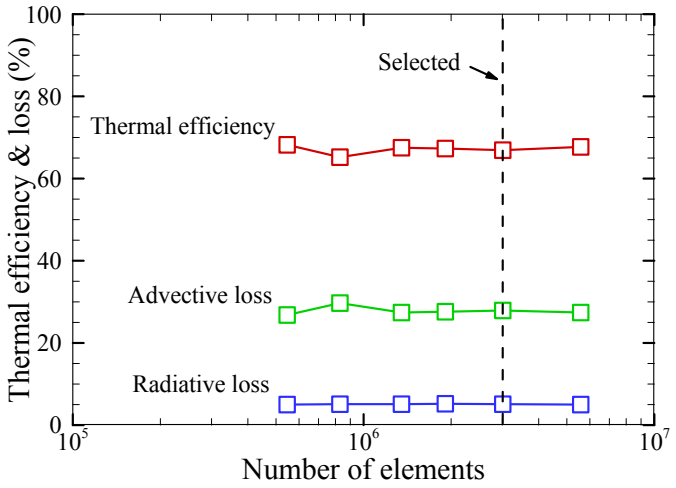

FIGURE 2. Grid-independence test in terms of thermal efficiency and advective/radiative losses for various spatial discretization. Vertical dashed line denotes the grid system chosen (3,008,286 elements).

MFPR GEOMETRY IN QUIESCENT CONDITION

The thermal efficiency of the receiver is used as the primary metric to evaluate the performance. The thermal efficiency is defined as:

$$\eta = \frac{Q_a}{Q_i} = \frac{\dot{m}\left(h_{o,p} - h_{i,p}\right)}{Q_i} = \frac{\dot{m}\int_{T_{i,p}}^{T_{o,p}} c_p(T)dT}{Q_i} \tag{1}$$

where Q_a is the thermal power absorbed by particles, Q_i is the incident thermal radiative power, h_p is the enthalpy of the particles, and $c_p(T_p)$ is the specific heat of the particles (J/kg·K) as a function of temperature defined using data from Georgia Tech's Thermophysical Properties Database:

$$c_p(T_p) = 388 \cdot T_p^{0.1523} \tag{2}$$

where T_p is the mean particle temperature.

The MFPR efficiency in a quiescent condition has been investigated. Fig.3(a) shows the solar irradiance profile on the aperture. In this study, the region where the radiative heat flux is greater than 90% of the maximum irradiance is defined as the 'hot-spot', S_{h1}, which is denoted by the white solid line in Fig.3(b). The y-range of S_{h1} is found as y_{h1} = [5.4m, 8.4m], which is denoted by the white dashed lines in Figs. 3(a) and (b). In Fig.3(b), the orange solid line denotes the projection of S_{h1} along the direction of incident solar radiation into the middle of the lower trough, S_{h2}.

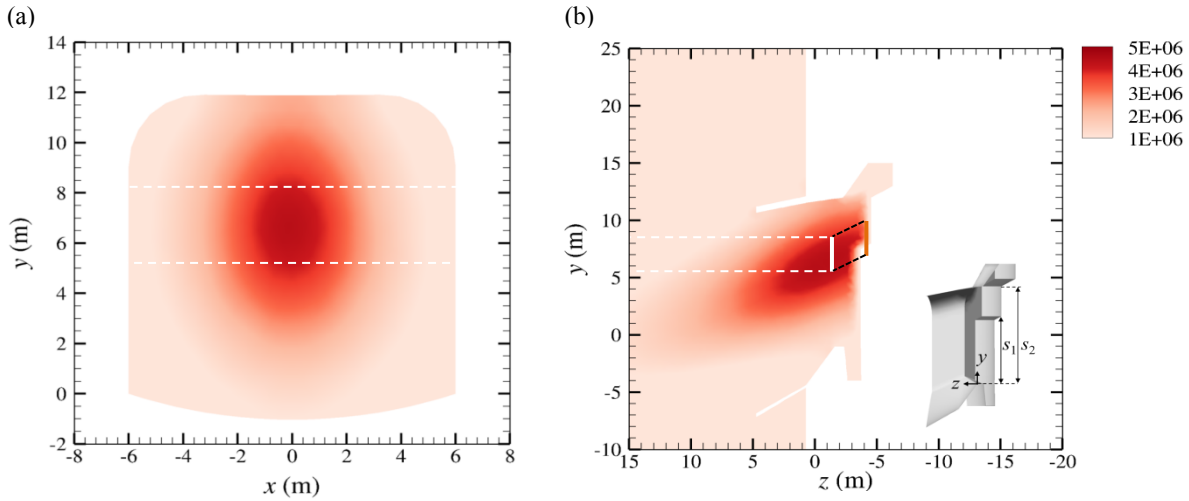

FIGURE 3. (a) Radiative heat flux profile at the aperture surface and (b) at y-z midplane for 2-stages MFPR with s_1=12m, s_2=8m, l_1=2m, l_2=1m, solar irradiance of 200 MW. The inset denotes the MFPR geometry. White solid line denotes the hot spot. Orange solid line denotes the projection of the hot spot along the direction of incident solar radiation into the middle of the lower trough. Black dashed lines indicate the projection lines. Contour map indicates the variation of thermal power (W/m²).

The receiver geometry is iteratively modified to maximize MFPR efficiency and surpass the quiescent FFPR efficiency of 83.2%. First, the thermal efficiencies are measured for a 2-stage MFPRs with trough lengths fixed to l_1=2m and l_2=1m. Fig.4(a) shows that for the upper trough height of s_1=12m, thermal efficiency increases with increasing lower trough height, s_2. As the position of the lower trough moves to S_{h2}, particles can absorb more energy from more highly concentrated solar radiation at S_{h2} for a longer duration. Particle residence time varies marginally within 7 – 7.5 seconds for s_1=12m, as shown in Fig.5, but the thermal efficiency does not show a consistent trend corresponding to the particle residence time in Fig.4(a). Rather, the time that particles reside at S_{h2} seems more related to the trends of thermal efficiency. Fig.5 shows that for the lower troughs located at s_2=8m and s_2=10m, falling particles reside near S_{h2} for longer duration compared to at s_2=4m and at s_2=6m. Increasing time that particles stay at S_{h2} enables the falling particles to absorb a greater amount of solar irradiance at a higher volume fraction, and thus it

results in improved thermal efficiency at s_2=8m and s_2=10m in Fig.4(a). This suggests that the intermediate troughs should be placed around the region where the solar irradiance is highly concentrated in order to maximize the thermal efficiency.

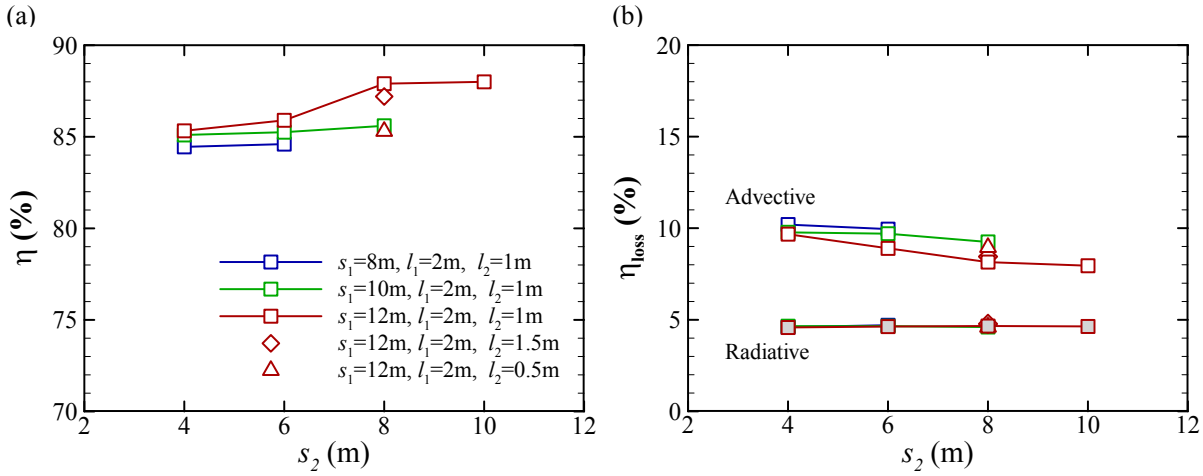

FIGURE 4. (a) Thermal efficiency and (b) thermal losses from radiative and advective losses for 2-stages MFPR in terms of various trough heights and trough lengths with incident solar power of 200 MW.

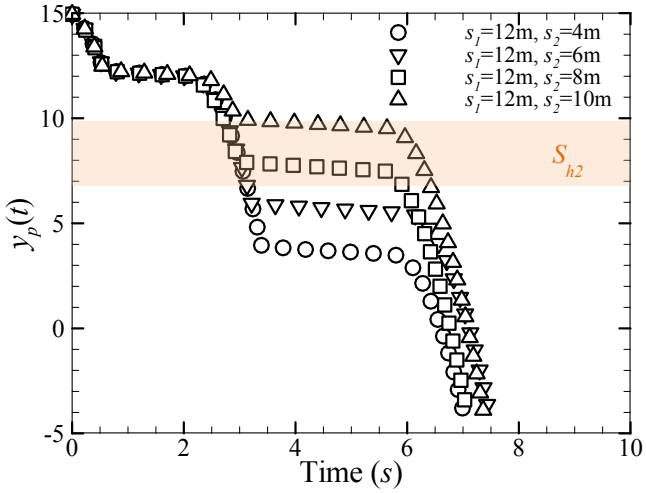

FIGURE 5. The y-position of particles as a function of time. The orange shaded region corresponds to the region denoted by orange solid lines in Fig.3.

The height of the upper trough can also affect the thermal efficiency. In Fig.4(a), the thermal efficiency decreases with lower s_1 for the same height of the lower trough. As the upper trough moves down, particle velocities are reset around S_{h2} as absorbing the heat energy from the highly concentrated sunlight. However, the particles can also encounter the cooler ambient air more easily as getting closer to the open aperture. Fig.4(b) shows that as s_1 decreases from 12m to 8m for the same height of the lower trough, advective losses increase.

Regarding the effects of the location of the troughs on the MFPR efficiency, the maximum thermal efficiency is achieved by minimizing the adverse effects from the ambient air entering the cavity and increasing time that particles absorb solar irradiance at S_{h2}. For consideration of the best performance, the tip of the upper trough is placed at s_1=12m, which is the same height of the upper edge of the open aperture. This places the upper trough away from the open aperture minimizing advective losses. In addition, the second lower trough is located at s_2=8m that enables the falling particle to absorb the heat energy from solar irradiance at S_{h2} for a long time. Moreover, increasing l_2 seems advantageous in comparison between l_2=0.5m and l_2=1m, but l_2 increasing over 1m does not seem critical to the

improvement of thermal efficiency as shown in Fig.4. Therefore, a 2-stage MFPR geometry is selected with s_1=12m, s_2=8m, l_1=2m, l_2=1m as the optimal MFPR geometry of this study. This MFPR geometry provides a thermal efficiency of 87.9%, which is 4.7% greater than FFPR efficiency in the quiescent condition.

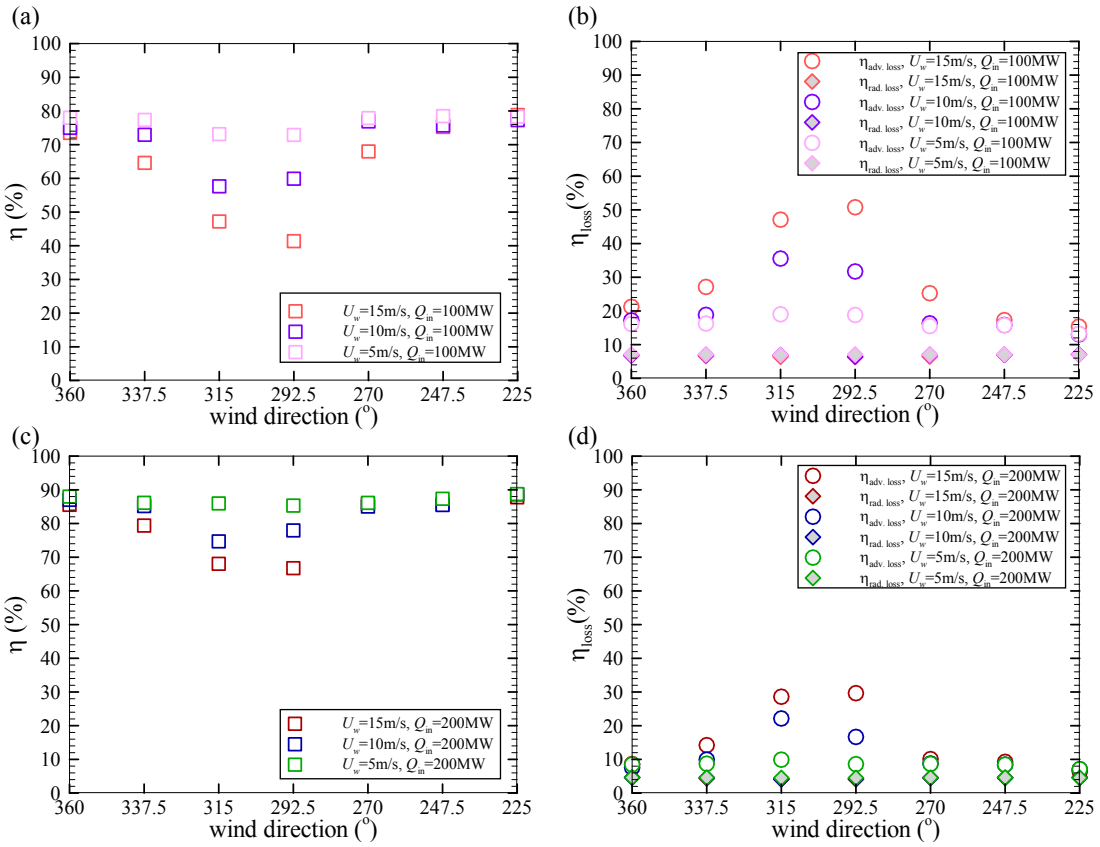

FIGURE 6. Thermal efficiency and thermal losses for various wind directions and speeds for incident solar power of 200 MW and 100 MW.

MFPR EFFICIENCY UNDER WIND EFFECTS

The MFPR efficiency has been evaluated with three separate wind speeds (5, 10, and 15 m/s), seven different wind directions (N, NNW, NW, WNW, W, and SW), and two different incident solar power (100 and 200 MW) in a parametric study. First, it is observed that thermal efficiency highly depends on the wind directions as also observed from previous studies [5]. Fig.6(a) and (c) show the thermal efficiency as a function of wind directions for various wind speeds and incident solar powers. North corresponds to wind direction of 0° or 360° and east corresponds to a wind direction of 90°. Advective losses vary significantly as a function of wind direction, however, the radiative losses change only marginally. As wind direction changes from N (0° or 360°) to NW (315°), the thermal efficiency decreases, and the advective loss increases. As wind direction changes from NW to SW, advective losses decrease and the thermal efficiency is recovered. This inverse relation between MFPR efficiency and advective loss indicates that the advective loss is the primary contribution in the degradation of the thermal efficiency in response to wind. The most detrimental condition comes from the wind blowing from either NW or WNW sides. For these wind directions, advective losses increase significantly due to the vortices that stimulate the advection between cooler ambient air and particle curtain as shown in Fig.7.

The MFPR efficiency is also affected by the wind speed. For a wind speed of 5m/s, the thermal efficiency varies within ~3% and ~6% at Q_i=100 MW and Q_i=200 MW, respectively. With increasing wind speed to 15m/s, the variation of thermal efficiency becomes significant. The thermal efficiency varies up to ~36% for Q_i =100 MW and ~29% for Q_i =200 MW, respectively. In addition, with increasing wind speed, the advective losses increase

significantly for either NW or WNW winds. This implies that increasing wind speed for NW or WNW winds intensifies the magnitude of vortices existing ahead of the open aperture, and thus the advection between cooler ambient air and particle curtain becomes more significant compared to low wind speeds.

Increasing incident solar power brings about an increase in the thermal efficiency and a decrease in the advective loss. This can be explained by the proportion of advective loss to the solar input power. The magnitude of the advective loss has marginal variability for different incident solar power at the same wind speeds and wind direction. However, the proportion of advective loss to solar input power is decreasing since the magnitude of heat energy absorbed by particle curtain increases and the magnitude of advective loss changes marginally. In other words, the percentage of the advective loss is decreasing, and thus the proportion of the energy being absorbed by falling particles is increasing. This is the reason why the thermal efficiency increases with higher incident solar power as shown in Figs. 6(a) and (c). Therefore, higher solar input power is desired as possible to maximize the efficiency under the effects of wind.

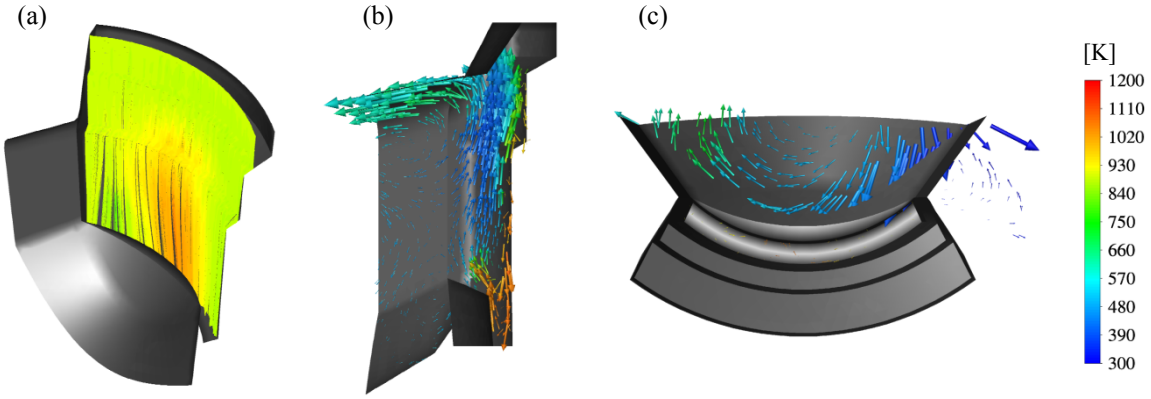

FIGURE 7. (a) 3D view of particle curtain inside MFPR cavity. (b) velocity vectors in *y-z* plane view and (c) *x-z* plane view for the case of wind direction: WNW and wind speed = 15m/s. Contour map indicates the temperature variation in [K].

CORRELATION DEVELOPMENT

A correlation of MFPR efficiency as a function of the incident solar power Q_i, the wind direction θ_w, and the wind speed U_w, has been developed from the simulation data provided with the advanced CFD model. 42 simulation cases are used to explore the relevant coefficients (*A, B, C, D, E,* and *F*) in terms of Q_i, Q_i^2, U_wG, $U_w^2G^2$, where G is the wind direction modifier which is used to provide more accurate fitting. The correlation function is as follows:

$$\eta_{cor} = A + BQ_i + CQ_i^2 + D(U_wG) + E(U_wG)^2 \tag{3}$$

where A=0.71967, B=2.60648×10^{-5}, C=−1.61945×10^{-4}, D=−0.0048123, E=0.229874. The coefficients are obtained using the generalized reduced gradient (GRG) nonlinear regression model, available in MS Excel. In this study, the wind direction modifier is defined as

$$G = \exp\left[-\left(\frac{|\theta_w - 180| - 123}{37}\right)^2\right] \tag{4}$$

The correlation of the MFPR efficiency derived from the parametric study shows good agreement with the MFPR efficiency predicted with CFD model as shown in Fig.8. In this study, an R-squared value of ~0.94 is obtained, indicating that the resulting correlation is sufficient to predict the thermal efficiency of a MFPR for system models.

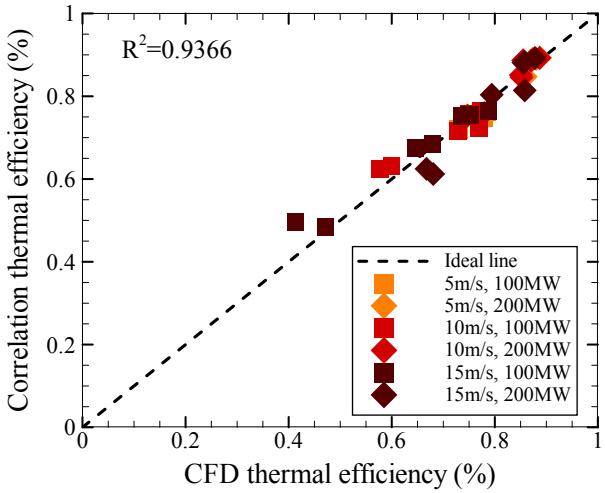

FIGURE 8. Parity plot of the CFD model and correlation thermal efficiencies colored by the measured wind direction and symbolized by the incident solar power.

CONCLUSIONS

The thermal efficiency of the proposed MFPR design for a 100 MW_e scale, particle-based CSP plant was evaluated in this paper. An advanced CFD model was developed to simulate MFPR efficiency. MFPR efficiency was first evaluated with trough lengths and trough heights in a quiescent condition. For consideration of the highest thermal efficiency, a 2-stage MFPR with the height of the upper trough of s_1=12m, the height of the lower trough of s_2=8m, the length of the upper trough of l_1=2m, the length of the lower trough of l_2=1m was chosen as an optimal MFPR geometry of this study. The best performing MFPR geometry provided the thermal efficiency of ~88%, which is ~4% greater than a similarly sized FFPR. With the selected MFPR geometry, MFPR efficiency was investigated for various wind directions, wind speeds, and incident solar powers. The inverse relation between the thermal efficiency and advective loss suggested that the advective loss was the key mechanism of performance degradation. The most detrimental condition came from the wind blowing from either NW or WNW sides with wind speed of 15m/s. In this case, vortical structures existing ahead of the open aperture intensified the advection between the ambient cooler air and the particle curtain, and thus the efficiency degradation became significant. Thermal efficiency with solar input power of 200 MW provided higher thermal efficiency compared to that of 100 MW, inspiring that the concentrated solar irradiance focused on the receiver should be as high as possible to maximize the thermal efficiency for a design. A correlation predicting MFPR performance was developed using a nonlinear regression fitting strategy available in MS Excel. The proposed correlation function enabled to predict the receiver efficiency as a function of wind, incident flux, and particle mass flow rate with R-squared value of ~94%. This correlation can be utilized in technoeconomic models to predict the LCOE under realistic operating and wind conditions.

ACKNOWLEDGMENTS

This work was funded in part or whole by the U.S. Department of Energy Solar Energy Technologies Office under Award Number 37372. This report was prepared as an account of work sponsored by an agency of the United States Government. Neither the United States Government nor any agency thereof, nor any of their employees, makes any warranty, express or implied, or assumes any legal liability or responsibility for the accuracy, completeness, or usefulness of any information, apparatus, product, or process disclosed, or represents that its use would not infringe privately owned rights. References herein to any specific commercial product, process, or service by trade name, trademark, manufacturer, or otherwise does not necessarily constitute or imply its endorsement, recommendation, or favoring by the United States Government or any agency thereof. The views and opinions of authors expressed herein do not necessarily state or reflect those of the United States Government or any agency thereof.

Sandia National Laboratories is a multi-mission laboratory managed and operated by National Technology and Engineering Solutions of Sandia, LLC., a wholly owned subsidiary of Honeywell International, Inc., for the U.S. Department of Energy's National Nuclear Security Administration under contract DE-NA0003525.

REFERENCES

1. Ho, C. K., "A review of high-temperature particle receivers for concentrating solar power," *Applied Thermal Engineering,* **109**, 958-969 (2016).
2. Albrecht, K. J., Bauer, M. L., Ho, C. K., "Parametric analysis of particle CSP system performance and cost to intrinsic particle properties and operating conditions", *Proceedings of the ASME 2019 13th International Conference on Energy Sustainability*, ES2019-3893 (2019)
3. Khalsa, S. S. S., Christian, J., Kolb, G. J., Röger, M., Amsbeck, L., Ho, C. K., Siegel, N. P., Moya, A. C., "CFD Simulation and Performance Analysis of Alternative Designs for High-Temperature Solid Particle Receivers", *Proceedings of the ASME 2011 5th International Converence on Energy Sustainability*, ES2011-54430 (2011)
4. Gobereit., B., Amsbeck, L., Buck., R., Pitz-Paal, Röger, M., Müller-Steinhagen., H., "Assessment of a falling solid particle receiver with numerical simulation", *Solar Energy*, **115**, 505-517 (2015)
5. Mills, B., Shaeffer, R., Ho, C. K., Yue, L., "Modeling the thermal performance of falling particle receivers subject to external wind", *Proceedings of the ASME 2019 13th International Conference on Energy Sustainability*, ES2019-3913 (2019)
6. Tan, T., Chen, Y, Chen, Z, Siegel, N. Kolb, G., "Wind effect on the performance of solid particle solar receivers with and without the protection of an aerowindow", *Solar Energy*, **83**,1815-1827 (2009)
7. Mills, B., Shaeffer, R., Yue, L., Ho, C. K., "Improving next-generation falling particle receiver designs subject to anticipated operating conditions", *Proceedings of the ASME 2020 14th International Conference on Energy Sustainability*, ES2020-1667 (2020)
8. Ho, C. K., Christian, J., Yellowhair, J., Siegel, N., Jeter, S., Golob, M., Abdel-Khalik, S. I., Nguyen, C., Al-Ansary, H., "On-sun testing of an advanced falling particle receiver system", *AIP Conference Proceedings*, **1734**, 030022 (2016)
9. Ho, C. K., Christian, J., Yellowhair, J., Armijo, K., Kolb, W. J., Jeter, S., Golob, M., Nguyen, C., "Performance evaluation of a high-temperature falling particle receiver", *ASME 2016 10th International Conference on Energy Sustainability collocated with the ASME 2016 Power Conference and the ASME 2016 14th International Conference on Fuel Cell Science, Engineering and Technology*, ES2016-59238 (2016)
10. Kim, J.-S., Kumar, A., Gardner, W., Lipinski, W., "Numerical and experimental investigation of a novel multistage falling particle receiver", *AIP Conference Proceedings*, **2126**, 030030 (2019)
11. Kumar, A., Lipinski, W., Kim, J.-S., "Numerical modelling of radiation absorption in a novel multi-stage free-falling particle receiver", *International Journal of Heat and Mass Transfer*", **146**, 118821 (2020)
12. Shaeffer, R., Mills, B., Yue, L., Ho, C. K., "Evaluation of performance factors for a multistage falling particle receiver", *ASME 2020 14th International Conference on Energy Sustainability*, ES2020-1692 (2020)
13. Siegel, N., Kolb, G., Kim, K., Rangaswamy, V., Moujaes, S., "Solid particle receiver flow characterization studies", *ASME 2007 Energy Sustainability Conference*, ES2007-36118 (2007)
14. Morsi., S. A., Alexander, A. J., "An investigation of particle trajectories in two-phase flow systems", *Journal of Fluid Mechanics*, **55**, 193-208 (1972)